Observed changes in fire patterns and possible drivers over Central Africa

IOP Publishing Environ. Res. Lett. 15 (2020) 0940b8 https://doi.org/10.1088/1748-9326/ab9db2

Environmental Research Letters

OPEN ACCESS

RECEIVED
11 December 2019

REVISED
26 May 2020

ACCEPTED FOR PUBLICATION
17 June 2020

PUBLISHED
11 September 2020

LETTER

Observed changes in fire patterns and possible drivers over Central Africa

Yan Jiang, Liming Zhou and Ajay Raghavendra

Department of Atmospheric and Environmental Sciences, University at Albany, State University of New York, Albany, NY 12222, United States of America

E-mail: yjiang6@albany.edu

Keywords: Central Africa, burned area, connected-component labeling,and machine learning

Supplementary material for this article is available online

Abstract

Fire is an integral part of Earth's system that links regional and global biogeochemical cycles, human activities, and ecosystems. Global estimates for biomass burning indicate that Africa is responsible for ~70% of global burned area and ~50% of fire-related carbon emissions. Previous studies have documented an overall decline in burned area in the African continent, but changes in fire patterns, such as the frequency and size of different fire categories, have not been assessed. In this study, long-term fire trends were investigated using the latest burned area data from the MODerate resolution Imaging Spectroradiometer (MODIS) and the Global Fire Emission Database (GFED4s) over Central Africa (10°E–40°E, 15°N–15°S). A 3D (latitude, longitude, time) connected-component labeling algorithm was applied to identify individual fires and their sizes. The results show a decline in burned area by 2.7–3.2 Mha yr^{-1} (~1.3% yr^{-1}) for the period 2003–2017, particularly in northern Central Africa. This decline was attributed to significant decreases in both fire frequency and size, particularly for large fires (>100 ha) which contribute to ~90% of the total burned area. Burned area declined in tropical savannas and grasslands but increased at the edges of the Congolese rainforest. A random forest regression model was applied to quantify the influences of climatic conditions, fuel availability, and agricultural activity on burned area changes. Overall, suppressed fuel, increased dry season length, and decreased rainfall contributed to significant declines in burned area in savannas and grasslands. At the edges of the southern Congolese rainforest, suppressed rainfall and warmer temperature were responsible for the increased burned area.

1. Introduction

Fires are an integral part of the Earth's system, interacting with climate, ecosystem, and human activities. Hot, dry, and windy conditions typically lead to severe fires (Jolly *et al* 2015). Humans influence fire regimes directly by igniting and suppressing fires but also indirectly by modifying the vegetation structure and composition (Lasslop and Kloster 2017). On the other hand, frequent fires are integral for savannas and grasslands, supporting a large range of endemic species, large mammals, and other wildlife (Scholes and Archer 1997). Inter-annual variability in wildfire extent largely drives variations in global carbon dioxide and aerosols (Patra *et al* 2005, Schultz *et al* 2008). Thus, understanding variations of fire regimes not only has implications for societal and economic developments but is also an urgent issue for studies on fire–climate–ecosystem interactions and fire prediction and management.

Though increasing wildfire risk is suggested under the warming and drying climate (Pechony and Shindell 2010), a complex big picture of prospective global and regional fire trends is emerging based on recent satellite observations (Aldersley *et al* 2011, Andela *et al* 2017). Increasing wildfire activity and burned area have been observed over the mid-latitude and subtropical forests in the Northern Hemisphere (Westerling *et al* 2006, Riaño *et al* 2007). In contrast, over the tropics, large decreases in burned area occurred in the savannas of South America, Africa, and grasslands across the Asian steppes (Andela *et al*

2017). On average, global burned area declined by 24% over the period 1996–2015, and there was a potential shift in global pyrogeography from savanna-dominated to forest-dominated (Andela *et al* 2017).

A holistic characterization of fire changes requires not only the consideration of the mean state of burned area but also variations in fire frequency and size. Fire frequency and size exert first-order impacts on biomass accumulations and land cover types (Yates *et al* 2009). Naturally, examining spatiotemporal variability in frequency and size of individual fires provides important information on changes in burned area. Previous studies suggested that decreased global burned area was mainly attributed to decreased fire frequency, while regional changes in fire frequency and size varied geographically (Andela *et al* 2017). Nevertheless, relatively few studies have examined the changes in frequency and size of different wildfire categories over the tropic hotspots.

Recent studies have documented regulations of weather or anthropogenic factors on wildfires by applying first-order linear statistic models (Flannigan *et al* 2009, Archibald *et al* 2010, Forkel *et al* 2019). One major challenge is determining the dominant factors that provide cross-scale insights for fire predictions under a changing climate (Archibald *et al* 2018). The complex interactions between fires, weather conditions and vegetation fuel make predictions difficult. Climatic and anthropogenic factors often show antagonistic and non-linear behaviors with respect to fire occurrence (Aldersley *et al* 2011). For instance, increased population density is associated with increased fire numbers, but it also reduces fuel load, which reduces fire spread (Lasslop and Kloster 2017). Recently, the random forest regression model has been applied to study drivers of fire to better interpret the explanatory nature of the independent variables (Archibald *et al* 2009, Aldersley *et al* 2011, Mayr *et al* 2018). This advanced model provides a promising new approach to deal with unprecedented amounts of data and to understand fire trends.

It is estimated that Africa is responsible for ~70% of global burned area and ~50% of fire-related carbon emissions, mostly from local savanna ecosystems (Andela and van der Werf 2014). Central Africa contains complex savanna, grassland and rainforest ecosystems and is a crucial hot spot for wildfires. It has experienced a long-term drying trend and a widespread increase in the boreal summer dry season length (DSL) since the 1980s (Zhou *et al* 2014, Hua *et al* 2016, 2018, Nicholson *et al* 2018, Jiang *et al* 2019), which may have exposed local ecosystems and societies to a greater risk of wildfires. The documented decrease in observed fires over Africa (Andela and van der Werf 2014, Andela *et al* 2017) based on the satellite-derived MODerate resolution Imaging Spectroradiometer (MODIS) Collection 5 burned area data suffered from large uncertainties, including the occurrence of false alarms caused by small forest clearings, the omission of large fires obscured by thick smoke and small fires by the limited algorithm, and sensor degradation (Giglio *et al* 2016).

The availability of an improved MODIS fire product provides a great opportunity to investigate robust trends in fires and possible drivers over Central Africa. The Collection 6 burned area mapping algorithm and product have several algorithmic improvements and calibration adjustments, which address the aforementioned data quality issues (Giglio *et al* 2018). This improved dataset also allows us to better separate contributions from different fire categories and different land cover types. With these in mind, we analyzed fire changes and possible drivers over Central Africa. Combining the utility of the random forest model, we aimed to answer the following questions: (i) Is there a decreasing trend in burned area over Central Africa as reported at the global scale? If yes, how does this change vary by land cover and attribute to changes in fire frequency and size? (ii) Which factors are primarily responsible for the changes?

2. Study region, data and methods

2.1. Study region

This study focused on Central Africa (10°E–40°E, 15°N–15°S). This domain was carefully chosen given that it has the highest fire frequency and the most extensive burned area in the world. Human influences vary from the minimum in the rainforest to the maximum in the savannas and grasslands (Zhou *et al* 2014). These features make Central Africa an ideal target to study the wildfire change in a warming climate and attribute human and climate drivers.

2.2. Satellite-retrieved burned area and land cover products

Two global satellite-derived burned area products were used. One was the monthly burned area variable at 500 m spatial resolution (MCD64A1 Collection 6, 2001–2018) combining the Terra and Aqua satellites from the National Aeronautics and Space Administration (NASA) (Giglio *et al* 2018). It provides the approximate date of burning by detecting changes in daily surface reflectance to study the size distribution of individual fires (Andela *et al* 2017). The Collection 6 algorithm offers better detection of small fires and detects about 20% more burned area in Africa (Giglio *et al* 2018). Burned area can be detected for many weeks after a fire has occurred and takes advantage of temporal and spatial structural changes in fires (Andela *et al* 2017). Since the Terra satellite was launched in December 1999 and the Aqua satellite was launched later in May 2002, the burned area trend combined from both satellites was quantified

from 2003–2017 to reduce instrumental uncertainties. Only pixels marked as valid observations by the pixel-level quality assurance (QA) information associated with the MCD64A1 dataset were used.

The other burned area product was the monthly Global Fire Emissions Dataset Version 4 (GFED4s, 1997–2016) at 0.25° spatial resolution (Randerson *et al* 2012, Giglio *et al* 2013). This product used the 500 m MCD64A1 Collection 5.1 product as its primary data layer and incorporated small fires using active fire detections from the Tropical Rainfall Measuring Mission (TRMM), Visible Infrared Scanner (VIRS) and Along-Track Scanning Radiometer (ATSR) (Giglio *et al* 2013).

Both the MODIS and GFED4s products depict a similar annual cycle of burned area (supplementary figure S1) (available online at stacks.iop.org/ERL/15/0940b8/mmedia). Burned area reaches the maximum in December north of the equator and in August south of the equator. A fire year was defined as five months before and six months after the peak fire month (Archibald *et al* 2009). The annual total burned area was calculated as three months before and four months after the peak fire month to include more than 90% of total burned area (van der Werf *et al* 2008). Then, the linear trend of annual burned area was estimated using ordinary least squares regression. A two-tailed Student's t-test was applied to assess whether the trend was statistically significant.

Next, the changes in burned area by land cover were examined. The annual MODIS land cover product (MCD12C1, 2001–2018) (Friedl and Sulla-Menashe 2015) at 0.05° resolution was used to identify the land cover type of each pixel in the study domain. There are 17 total land cover types classified based on the International Geosphere–Biosphere Programme (IGBP) classification scheme (supplementary table S1). Seven major land cover types including evergreen broadleaf forest, deciduous broadleaf forest, mixed forest, woody savanna, savanna, grassland, and croplands (including croplands with natural vegetation mosaics) cover up to 97% terrestrial area of the study region (supplementary table S1 and figure S2), and about 96% burned area has occurred in these seven land cover types. The land cover type for each burning pixel was first assigned using the MCD12C1 and then the total burned area for each of the seven land cover types was spatially aggregated. Thus, the burned area in the study region was divided into seven sub-regions by land cover.

2.3. Connected-component labeling

A 3D (latitude, longitude, time) connected-component labeling (CCL) algorithm was adopted to identify individual fires (Archibald and Roy 2009, Hernandez *et al* 2015, He *et al* 2017). It labels an individual fire based on the following rules. First, a fire ID is given to the first burned pixel when all pixels begin as unclassified. Then, pixels neighboring this labeled pixel including diagonals (eight possible neighbors) are identified. If any of these pixels are recorded as burned within 8 days of the date when the central pixel burns, they are labeled with the same fire ID. (Archibald and Roy 2009). The CCL algorithm was repeated until all burned pixels were allocated with an individual fire ID. Eight days was used as a cut-off given the temporal duration window of the original MODIS data (Giglio *et al* 2018). Fire events were categorized into six different types: <100 ha (1 km^2, small fire), 100–500 ha, 500–1000 ha, 1000–10 000 ha, 10 000–50 000 ha and >50 000 ha (Archibald and Roy 2009). Due to the limited spatial resolution of the MODIS product, fires smaller than 25 ha were not considered in this study. Linear trends and their statistical significance in fire frequency and size were calculated in the same manner as the annual burned area detailed in section 2.2.

2.4. Random forest regression model

A random forest regression model was applied to study drivers of burned area variations in three land cover types (savannas, grasslands, and evergreen forest) that showed strong interannual variations and trends in burned area (see more in section 3.3). A single regression tree is a hierarchical classifier that predicts class membership by recursively partitioning data into more homogeneous subsets without assumptions concerning the statistical distribution of the data. However, a single output tree is sensitive to small differences in input datasets (Aldersley *et al* 2011). As a bootstrapping procedure, random forest grows a bunch of regression trees to improve the predictive ability of a single regression tree and reduce overfitting. Details regarding the spatially resolved data used in the model and the random forest sets are described next.

Nine variables were included in the conceptual model as predictors based on previous studies (table 1). Annual precipitation (P) and DSL were calculated by the three-hourly TRMM (3B42) precipitation product (Huffman *et al* 2007). Annual precipitation was calculated starting 12 months before the peak fire month up to and including the peak fire month (total 13 months) (van der Werf *et al* 2008). Daily rainfall estimates during a fire year within each grid were ranked and summed in descending order until at least 98% of annual rainfall was reached. The remaining number of days was the length of the dry season for that pixel (Guan *et al* 2018). The 98% threshold was chosen to consider highly varied rainfall seasonality over different ecological regions in Central Africa (Jiang *et al* 2019). Fuel availability was quantified by the biweekly MODIS Terra normalized difference vegetation index (NDVI) product at 0.05° resolution (MOD13C1, 2000-present) (Didan 2015).

Table 1. Datasets of variables used as predictors in the random forest model.

Variables	Time	Spatial resolution	Temporal resolution	Dataset
precipitation (P) dry season length (DSL)	1998–present	0.25°	3-hourly	TRMM 3B42
NDVI	2000–present	0.05°	biweekly	MOD13C1
tree cover	2003–2017	250 m	yearly	MOD44B
surface wind speed	1980–present	0.625° × 0.5°	monthly	MERRA-2
surface air temperature	1980–present	0.625° × 0.5°	monthly	MERRA-2
surface specific humidity	1980–present	0.625° × 0.5°	monthly	MERRA-2
number of thunderstorm events	1982–2016	0.07°	3-hourly	GridSat-B1
cropland extent	2001–2018	0.05°	yearly	MCD12C1

A high NDVI value indicates sufficient biomass favoring burning. The annual 250 m MODIS tree cover product (MOD44B, 2003–2017) (Dimiceli *et al* 2015) was applied as well. Large tree cover is adverse for grass growth and thus reduces the accumulation of biomass supporting burning (Laris 2011).

Climate conditions, including surface wind speed, surface air temperature and specific humidity, from the monthly Modern-Era Retrospective Analysis for Research and Applications, v.2 (MERRA-2, 1980–present) at 0.625° × 0.5° resolution were used (Gelaro *et al* 2017). Monthly mean weather variables during the fire season were calculated. Lightning strikes are a prominent ignition source (Aldersley *et al* 2011). It was indirectly measured by monthly thunderstorm frequency using the three-hour gridded infrared (IR) channel brightness temperature (T_b) dataset at 0.07° resolution (GridSat-B1, 1982–2016; Knapp *et al* 2011). T_b ranging between −40 and −70 °C was used to quantify thunderstorm activity in tropical latitudes (Raghavendra *et al* 2018). Since total climatological lightning flash rates correspond well to changes in the number of storms (Williams *et al* 2000, Cecil 2015), thunderstorm event records provide reliable information about lightning strikes.

Human activities affect fuel load and continuity as well as ignition frequencies (Archibald *et al* 2009). However, anthropogenic factors were limited to cropland extent in this study due to the lack of continuous records for road nets and population density. Cropland extent variations in different land cover types were calculated from the MODIS land cover product to quantify the impacts of agricultural expansion on fires. For easier comparison, all datasets used in this study were remapped on a 0.25° grid box using nearest-neighbor resampling.

Grids with significant ($p < 0.1$) burned area trends were classified into low ($< 30^{th}$ percentile) and high ($> 70^{th}$ percentile) burned area to conduct the random forest analysis. There are fewer fires in the rainforest, so we extended the definition of high burned area ($> 65^{th}$ percentile) to enlarge the training data size. First, all datasets, including burned area, were randomly partitioned into training (90% of total data) and test (10% of total data) datasets in the random forest model. Then, 1000 trees were grown to guarantee model stabilization. Each tree used a different random bootstrap subset of predictor and burned area variables (about 66% of the training sets). For split conditions at each node, one third of the total number of predictor variables (i.e. three out of nine variables) were recommended based on the estimate of the Gini impurity (Breiman and Cutler 2003). No further splitting was performed when nodes had fewer than five cases (Breiman 2001). The accuracy of the random forest regression was assessed by two methods (Breiman 2001, Mayr *et al* 2018). One is the out-of-bag score, which calculates the squared correlation coefficient between the burned area predicted by the model trained by the 66% training sets and observations from the rest of the training sets (33%). The other method calculates the Pearson correlation coefficient between the burned area predicted by the test datasets and the model and observed burned area. The results provide relative contributions of individual physical variables and their critical values favoring or suppressing fire activities.

3. Results

3.1. Trends of annual burned area

Annual mean burned area is shown in figures 1(a)–(b). There is a high level of burned area over northern Central Africa (including the Central African Republic and southern Sudan) and southern Central Africa (including Angola and southern Democratic Republic of Congo) but less burning over the wet Congo rainforest in general. The maximum annual mean burned area reaches 96% within in a single grid box in northern Central Africa estimated by both burned area products.

Figures 1(c)–(d) display the spatial patterns of burned area trends from MODIS (2003–2017) and GFED4s (2003–2016). In northern and northwestern Central Africa, there is a significant negative trend ($p < 0.05$) in burned area, with a maximum decreasing rate of about 2% yr^{-1}. A mild, decreasing trend exists in southern Central Africa and parts of the Ethiopian highlands in the east. A significant increase in burned area occurs in the southwestern and northwestern edges of the Congo rainforest as well, which

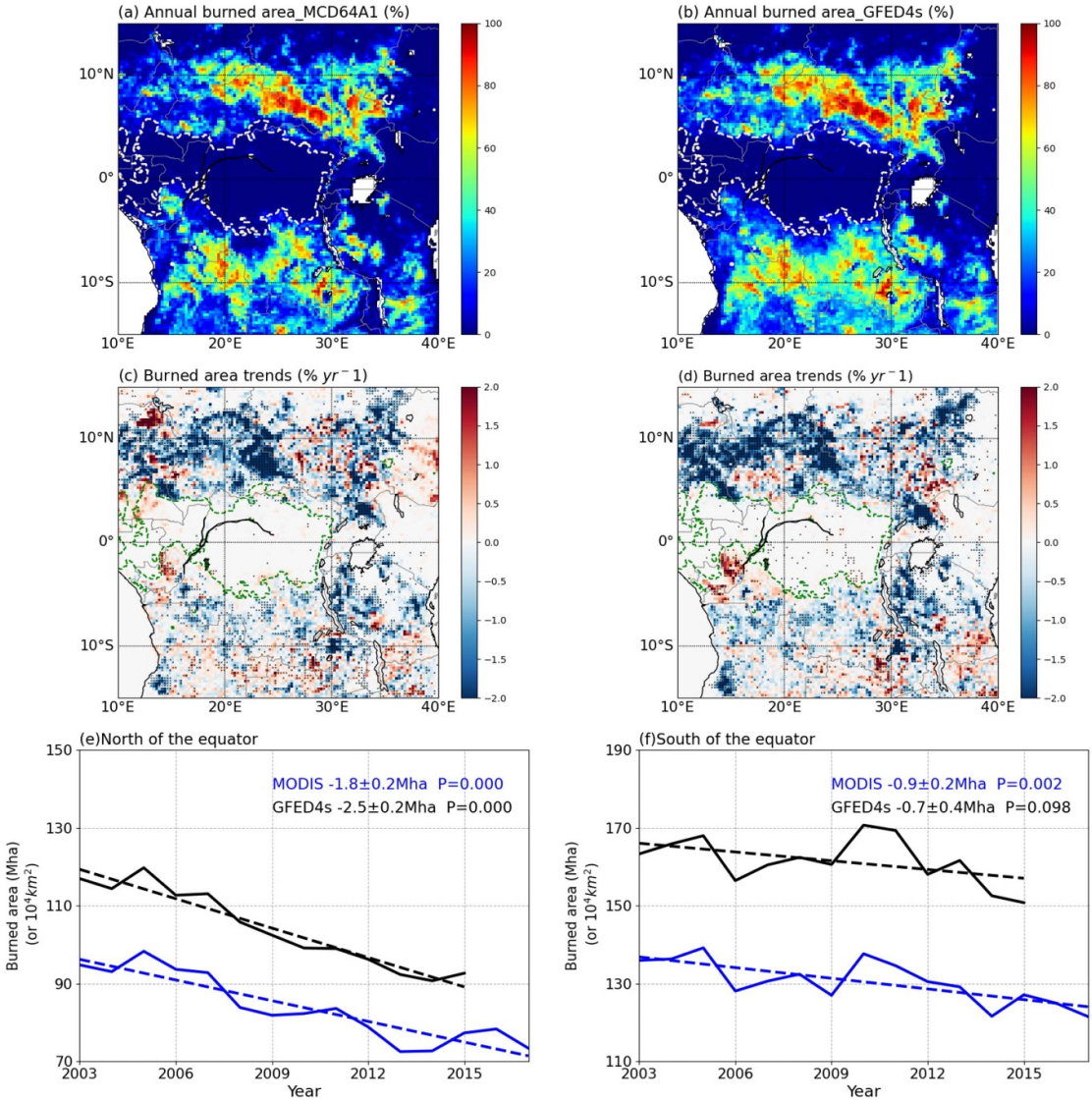

Figure 1. Spatial patterns of annual mean burned area from (a) MODIS and (b) GFED4s, and linear trends of annual mean burned area for the period 2003–2016/17 from (c) MODIS and (d) GFED4s. The dashed line delineates the boundary of the Congolese rainforest. Grid boxes with black dots have a significant trend at $P < 0.05$. Regionally aggregated interannual variations (solid line) and linear trends (dashed line) of annual mean burned area: (e) north and (f) south of the equator estimated from the MODIS and GFED4s. The linear trend and its significance level P are shown.

highlights the increasing risk of wildfire leakage into the rainforest.

Figures 1(e)–(f) show the interannual variations in burned area spatially averaged over northern and southern Central Africa. Though the GFED4s data detected more annual burned area than the MODIS data, both products observed similar interannual changes in burned area. The annual burned area has decreased dramatically by 1.8–2.5 Mha (10^4 km^2) yr^{-1} ($P = 0.00$) in the north, particularly over tropical savannas and grasslands. Burned area decreased at a lower rate by 0.7–0.9 Mha yr^{-1} ($p < 0.1$) in the south.

3.2. Changes in fire frequency and size

The histograms of fire frequency are shown in figure 2(a). Small fires (<100 ha) contribute to 66% and 64% of total fire numbers north and south of the equator, respectively. Mega fires (>1000 ha) only count for about 5% in the north and 4% in the south. The annual fire frequency has decreased in the north at a rate of 2000 yr^{-1} (about 0.75% yr^{-1}), while it has varied little in the south (figures 2(b)–(c)). The significant decline in fire frequency in the north was mainly attributed to dramatic decreases in large fires (>100 ha). Fires larger than 500 ha have decreased at a rate of about 1.5% per year, and small fires have also slightly decreased at a rate of about 0.5% (figure 2(d)). Though there was no significant trend in fire frequency in the south, decreases also occurred with large fires larger than 1000 ha (figure 2(e)).

Next, changes in fire size were studied. In general, small fires contribute to 7.6% and 10% of total burned area in the north and south, respectively. Though large fires only count for about 30% of total fire events, they contribute up to about

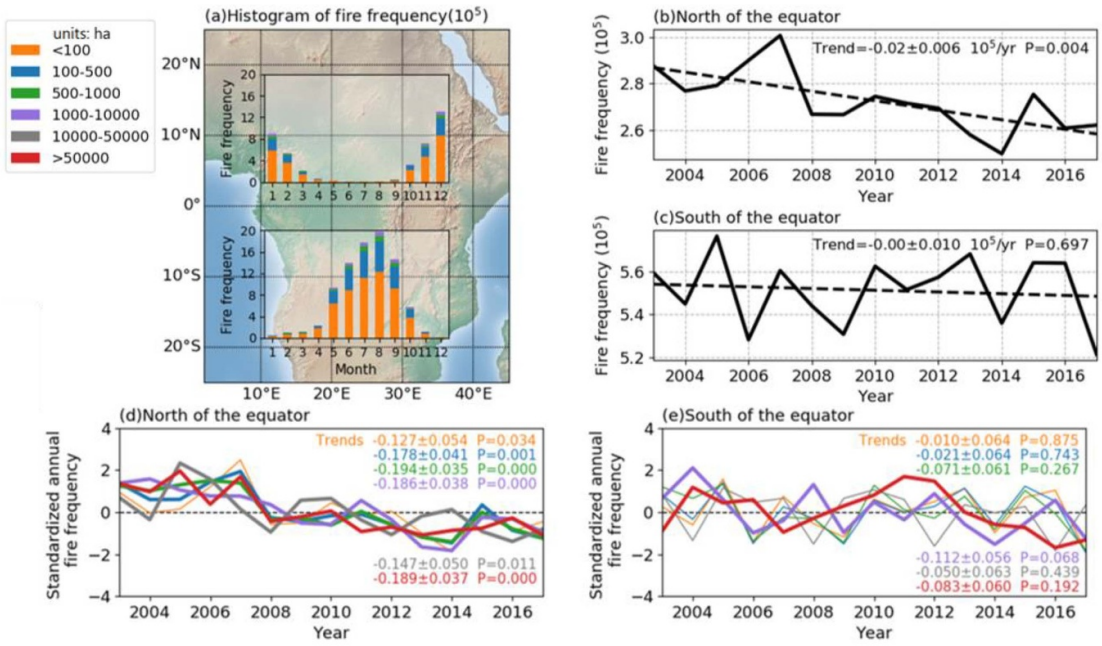

Figure 2. Histogram and variations of fire frequency over Central Africa estimated by the MODIS product for the period 2003–2017. (a) Histogram of fire frequency for different fire categories. Interannual variations and linear trends of total fire frequency (b) north and (c) south of the equator. Interannual variations and linear trends of standardized fire frequency in different categories (d) north and (e) south of the equator. Linear trends and significance levels are shown.

90% of the total burned area (figure 3(a)). Significant decreases in the mean size of different fire categories have occurred in the north, particularly for mega fires larger than 50 000 ha for which size decreased by 1.6% yr^{-1} (figure 3(b)). Small fires have slightly decreased by about 0.2% yr^{-1}. Mild, but non-significant, decreasing trends in large fire size have happened in the south as well (figure 3(c)).

3.3. Dependence of burned area changes on land cover types

Most fires happened over savannas (about 53%) and grasslands (about 30%), particularly in the north (figure 4(a)). A small percentage of burned area occurred over forested regions (about 10%) in the south (figure 4(a)). The long-term trends in annual burned area within savanna and grassland ecosystems are shown in figures 4(b)–(c). Burned area has decreased significantly by 1.41–1.77 Mha yr^{-1} ($p < 0.01$) for the period 2003–2017 in the north and decreased by 0.48–0.83 Mha yr^{-1} in the south. Decreases in burned area in savannas and grasslands substantially contributed to the total decline in burned area in Central Africa (70%–80% in the north, 69%–89% in the south). Though only about 4% burned area occurred in croplands, burned area decreased significantly by 0.31–0.53 Mha yr^{-1} ($p < 0.01$) in croplands north of the equator.

Figures 4(d)–(e) show the interannual variations in burned area in forested regions. Annual burned area slightly decreased by 0.07–0.08 Mha yr^{-1} in the north. Conversely, it increased significantly by 0.13–0.15 Mha yr^{-1} ($p < 0.05$) in the south. The increased burned area in forested regions was mainly attributed to increased burned area over mixed forests. In particular, burned area increased in the rainforest edges by 0.012 Mha yr^{-1} ($p = 0.15$) (about 1.14% yr^{-1}) according to the MODIS product. To disentangle drivers of burned area changes in savannas, grasslands and rainforest edges, the random forest regression was applied next.

4. Possible drivers of burned area changes

First, all potential variables affecting burned area were assessed by calculating the climatological mean values for the period 2003–2017 over savannas and grasslands, and rainforest edges (supplementary table S2). Savannas and grasslands, with more burnings and significantly decreasing burned area trends, are characterized by higher precipitation, shorter DSL and higher 2-m temperature during the fire season. The southern edge of the Congo rainforest, with a positive burned area trend, is characterized by a lower precipitation amount and longer DSL. Distributions of burned area grids in savannas and grasslands show that the decreasing burned area in savannas and grasslands may be attributed to a decrease in the occurrence of high burned area and an increase in the occurrence of low burned area (supplementary figures S3(a)–(b)). These results are consistent with the decreasing trends in the frequency and size of large fires. The increasing burned area over the southern Congolese rainforest edges may be attributed to an increase in the occurrence of high burned area (supplementary figure S3(c)).

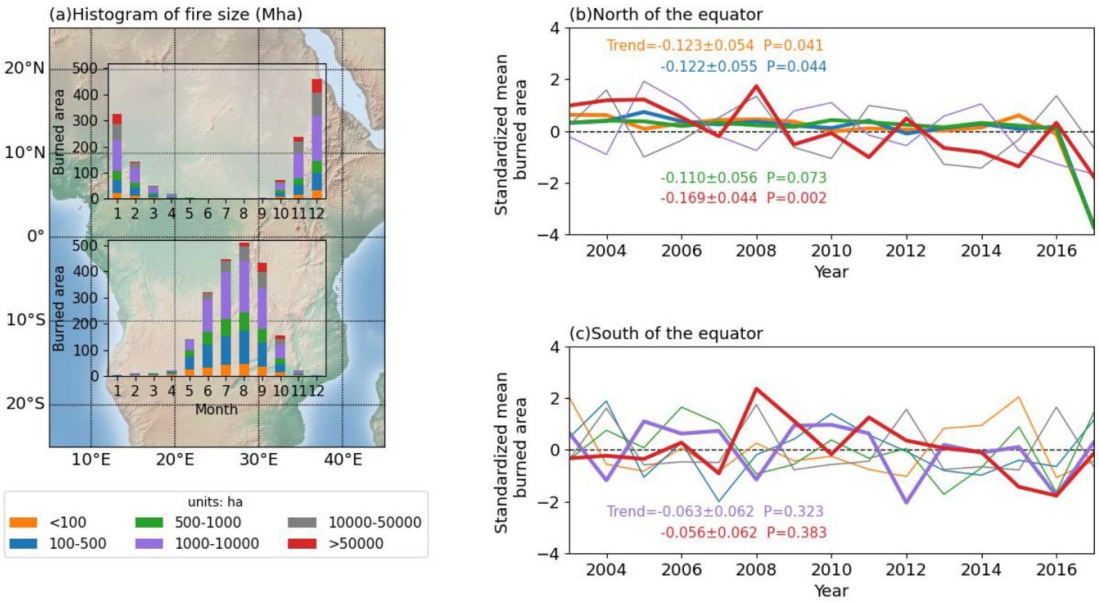

Figure 3. Histogram and variations of fire size over Central Africa estimated by the MODIS product for the period 2003–2017. (a) Histogram of contributions from different fire categories to total burned area. Interannual variations and linear trends of standardized mean fire size in different categories (b) north and (c) south of the equator. Linear trends and significance levels are shown.

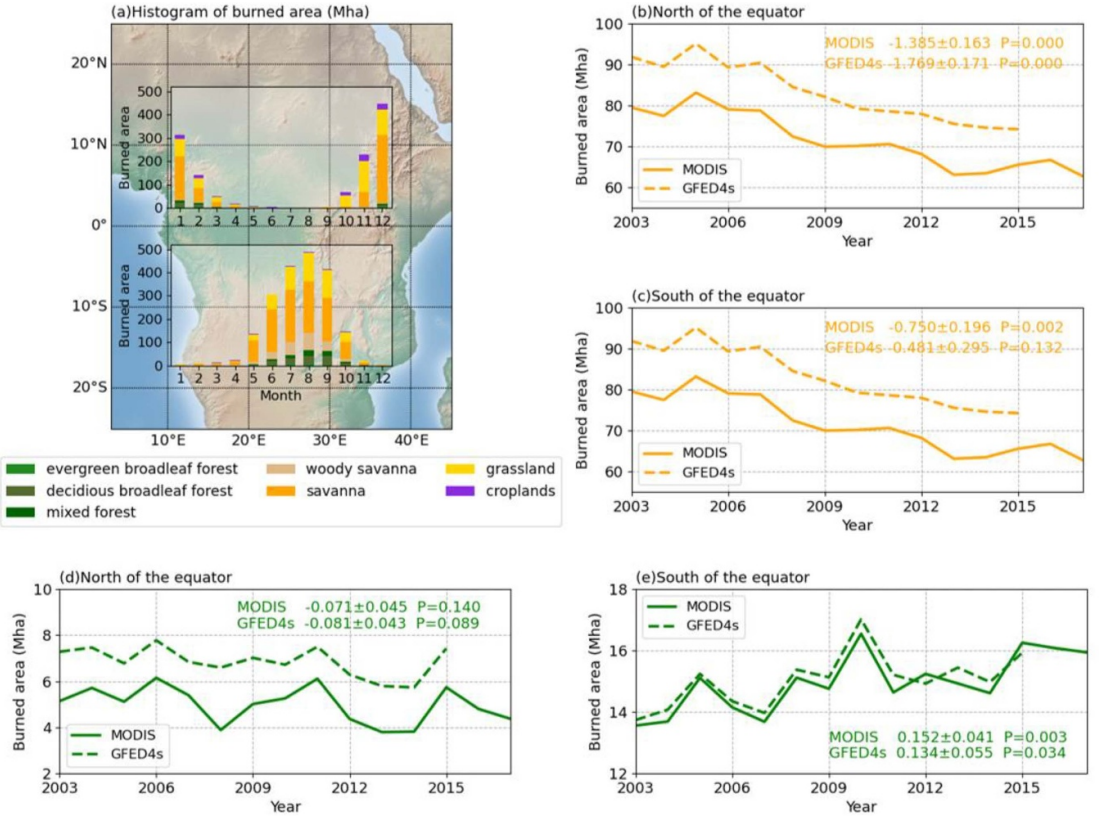

Figure 4. Histogram and variations of burned area in different land cover types over Central Africa estimated by the MODIS and GFED4s for the period 2003–2017. (a) Histogram of burned area for different land cover types. Interannual variations (solid line) and linear trends (dashed line) of burned area in savannas and grasslands (b) north and (c) south of the equator. Interannual variations and linear trends of burned area in forested regions (d) north and (e) south of the equator. Linear trends and significance levels are shown.

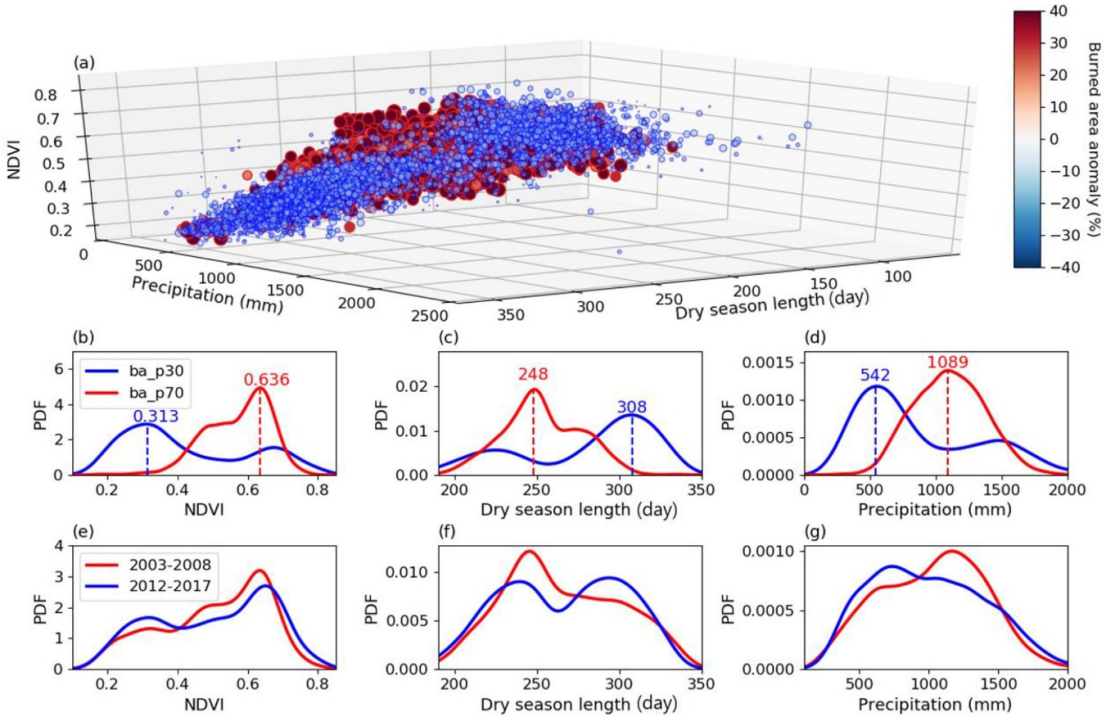

Figure 5. Relationships between annual burned area from MODIS and NDVI, dry season length (DSL), and precipitation amount over savannas and grasslands in the northern hemisphere for the period 2003–2017. (a) NDVI versus precipitation amount and DSL against burned area. Small circles shaded in blue represent low burned area. Large circles shaded in red represent high burned area. Probability density functions (PDFs) of (b) NDVI, (c) DSL, and (d) precipitation amount for high (red) and low (blue) burned area. The critical values are marked. Comparisons of (e) NDVI, (f) DSL and (g) precipitation between 2003–2008 (red) and 2012–2017 (blue). PDFs are calculated by kernel density estimation (KDE) to demonstrate the distribution of the variable. 'ba_p30' and 'ba_p70' refer to burned area lower than the 30th percentile and higher than the 70th percentile of all burning grids, respectively.

According to the random forest analysis, NDVI ranks as the most important variable and is followed by DSL and precipitation in northern savannas and grasslands (supplementary table S3). Grids with a higher NDVI value, shorter DSL and higher precipitation amount are favorable for high burned area (figures 5(a)–(d)). The random forest model characterized the training dataset well, with high out-of-bag correlation ($R_o = 0.91$), and predicted burned area using the test datasets with a high Pearson correlation coefficient ($R_p = 0.81$, $p = 0.00$). Comparisons between the composites of the three most important variables between 2003–2008 and 2012–2017 indicate that the decrease in the number of grids with high burned area is attributed to decreasing NDVI values and precipitation amount and increasing DSL (figures 5(e)–(g)). Positive correlation was observed between precipitation and NDVI ($R = 0.83$, $p = 0.0$), and negative correlation existed between DSL and NDVI ($R = -0.87$, $p = 0.0$). These results are consistent with previous studies indicating that lower moisture availability in arid or semi-arid ecosystems can decrease fuel build-up and burned area in the following years over longer time scales (van der Werf *et al* 2008, Archibald *et al* 2010, Bistinas *et al* 2014, Lehmann *et al* 2014).

The random forest model worked well for savannas and grasslands in the south with $R_o = 0.88$ and $R_p = 0.74$ ($p = 0.00$). NDVI, DSL and surface specific humidity are the three most important variables influencing fires. Similarly, a higher NDVI value and shorter DSL favor high burned area (figures 6(a)–(d)). Depending on the scenario, both positive and negative specific humidity anomalies can favor burning. Low humidity dries out plants, increasing the flammability of fuel. High humidity favors plant growth, increasing the amount of fuel. The mild decreasing trend in high burned area was mainly attributed to a decreased NDVI, longer dry season and slightly drier conditions (figures 6(e)–(g)). Longer DSL suppresses the accumulation of fuel, as seen by the negative correlation ($R = -0.57$, $p = 0.0$) between DSL and NDVI.

The random forest model was applied to the southern Congolese rainforest edge as well. Precipitation amount, surface wind speed and temperature significantly affect burned area ($R_o = 0.83$ and $R_p = 0.63$). Precipitation around 1585 mm, 10-m wind speed around 5.5 m s^{-1} and temperature around 295.3 K during the fire season facilitate fire activities (figures 7(a)–(d)). The increasing high burned area at the southern edge of the Congo

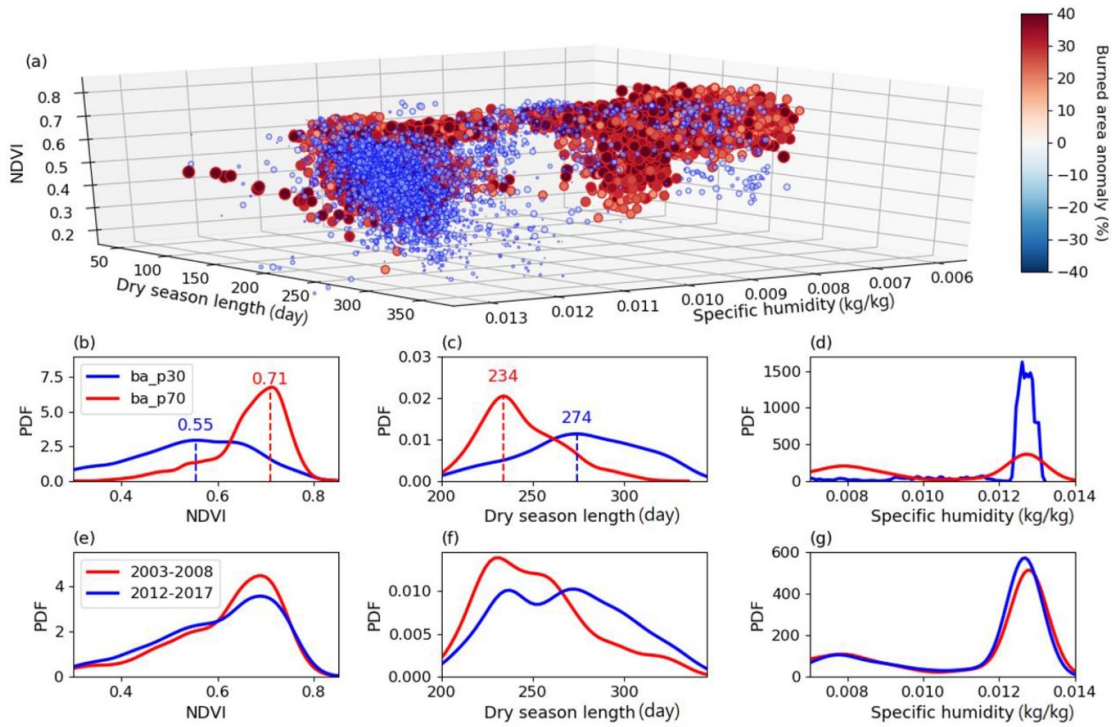

Figure 6. Relationships between annual burned area from MODIS and NDVI, DSL, and specific humidity over savannas and grasslands in southern hemisphere for the period 2003–2017. (a) NDVI versus DSL and specific humidity against burned area. Small circles shaded in blue represent low burned area. Large circles shaded in red represent high burned area. Probability density functions of (b) NDVI, (c) DSL and (d) specific humidity for high (red) and low (blue) burned area. The critical thresholds are marked. Comparisons of (e) NDVI, (f) DSL, and (g) specific humidity between 2003–2008 (red) and 2012–2017 (blue). 'PDF', 'ba_p30' and 'ba_p70' are defined as in figure 5.

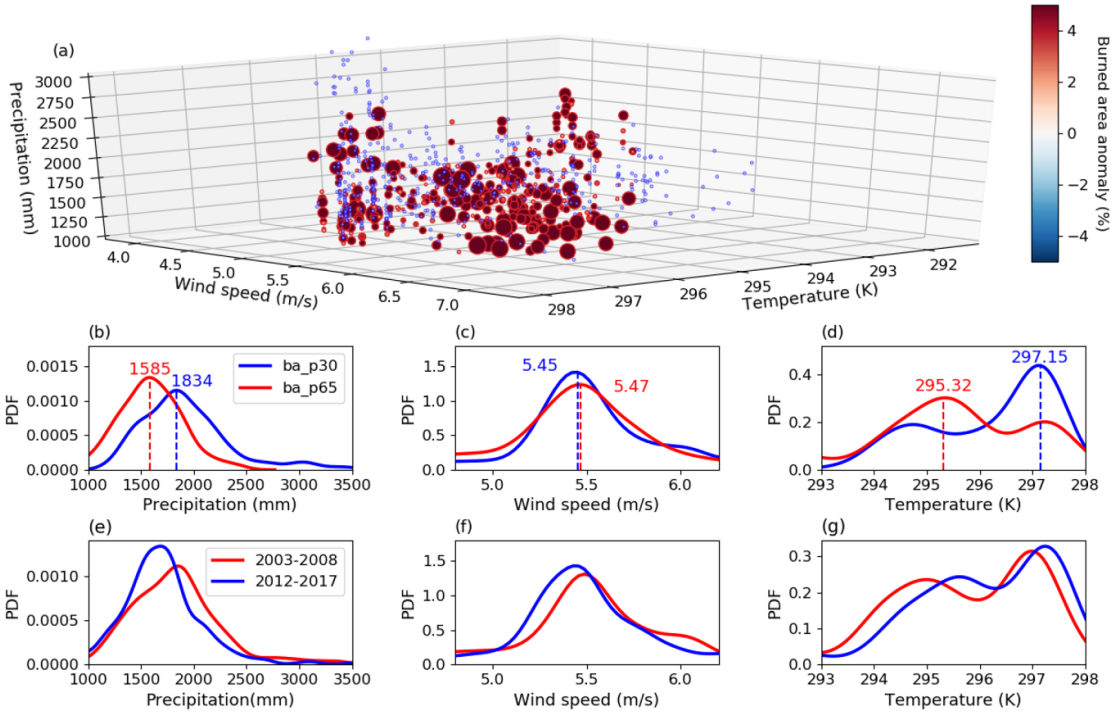

Figure 7. Relationships between annual burned area from MODIS and precipitation amount, wind speed and temperature in the southern rainforest edges for the period 2003–2017. (a) Precipitation amount versus wind speed and temperature against burned area. Small circles shaded in blue represent low burned area. Large circles shaded in red represent high burned area. Probability density functions of (b) precipitation amount, (c) wind speed and (d) temperature for high (red) and low (blue) burned area. The critical thresholds are marked. Comparisons of (e) precipitation amount, (f) wind speed and (g) temperature between 2003–2008 (red) and 2012–2017 (blue). 'PDF' and 'ba_p30' are defined as in figure 5. 'ba_p65' refers to burned area higher than the 65th percentile of all burning grids.

rainforest is attributed to reduced precipitation and increased temperature (figures 7(e)–(g)).

5. Discussions and conclusions

Using advanced satellite observations, we found that burned area has decreased by 2.7–3.2 Mha yr^{-1} since the early 2000s in Central Africa. While previous analyses documented downward trends in the north but upward trends in the south (Andela *et al* 2017), our results indicate that burned area has declined in both northern and southern Central Africa. Both fire frequency and size have declined, particularly for large fires (>100 ha) in the north. In addition, the decrease in fire frequency slightly outweighs the decrease in fire size.

Most of the burned area and decreased burned area trends occur in the savannas and grasslands. The highest levels of fire activities observed in the savanna ecosystems are characterized by intermediate levels of precipitation and distinct wet and dry seasons favoring fuel build-up and dry-out (van der Werf *et al* 2008, Andela and van der Werf 2014). Most of the fire emissions originate from the savanna ecosystems and exert strong effects on atmospheric carbon dioxide and methane concentrations, which are crucial climate drivers (van der Werf *et al* 2010). Decreases in the frequency of large fires and burned area in tropical savannas and grasslands may support global warming mitigation by acting as a carbon sink but would run counter to conservation objectives in fire-dependent ecosystems. Increasing burned area in forested areas was observed in the south, including the edge of the southern Congolese rainforest. The local intact rainforest has become increasingly fragmented since 2001 (Potapov *et al* 2017). Forest edges are often juxtaposed with frequently burned pastures and degraded by selective deforestation (Cochrane and Laurance 2002). Increased burning may initiate a positive loop, which augments the rainforest fragmentation and affects its carbon storage (Cochrane *et al* 1999, Nepstad *et al* 1999).

We used the MODIS and GFED4s burned area products in this study. Boosted by better fire mapping algorithms, both burned area products have been improved to detect small fires. The MODIS product also provided information about changes in different categories of fires. Nevertheless, smaller fires <25 ha were not included due to the constraint of image spatial resolution. Poor measurements of these small fires would introduce large uncertainties when studying fire variations in regions such as croplands where smaller fires are relatively important (van der Werf *et al* 2017, Giglio *et al* 2018). These sub-grid small fires are likely to increase total burned area and carbon emissions by 35% globally (Randerson *et al* 2012). Though it is impossible to quantify the contribution of these smaller fires to total burned area and fire events, our results for fires between 25 and 100 ha in Central Africa suggest that this contribution is non-negligible to fire events but may be minor to total burned area. In addition, the diurnal cycle of individual fires cannot be documented by the fire products due to the constraint of image temporal resolution. Though the overall burned area trends were comparable from both the MODIS and GFED4s products, knowing more details about sub-grid fires and individual fire evolutions would facilitate our understanding of burned area changes and their physical mechanisms.

Our random forest analysis analytically revealed that the decreasing trend of burned area in savannas and grasslands was mainly attributed to changes in precipitation activities and vegetation fuel. A positive correlation between precipitation and NDVI and a negative correlation between DSL and NDVI indicate that moisture availability is crucial for fuel build-up in these semi-arid ecosystems. The decreased high burned area was mainly attributed to longer DSL, decreased precipitation and suppressed fuel build-up. Decreased precipitation and increased temperature were responsible for increased burned area at the southern rainforest edge. Increased agricultural activities were considered as the primary drivers of declining fire activities in the tropics and subtropics (Malhi *et al* 2008, Andela *et al* 2017). The machine learning method highlights the impacts of vegetation fuel and weather factors on local wildfire variability under the changing climate. To better examine anthropogenic effects on fires, additional continuous records of population density, road density, and grazing intensity are required. Detailed vegetation–fire interaction and explicit physical mechanisms need further study via advanced land model simulations and causality analysis.

Acknowledgments

This study was supported by the National Science Foundation (NSF AGS-1535426 and AGS-1854486). The authors declare no competing interests.

Data availability statement

The data that support the findings of this study are openly available at the following URL/DOI: https://lpdaac.usgs.gov/. The MODIS burned area, land cover, and tree cover datasets are openly available at https://lpdaac.usgs.gov/. MERRA-2 reanalysis data can be obtained from the Goddard Earth Sciences Data and Information Services Center. GridSat-B1 brightness temperature data are available at https://www.ncdc.noaa.gov/gridsat/.

References

Aldersley A, Murray S J and Cornell S E 2011 Global and regional analysis of climate and human drivers of wildfire *Sci. Total Environ.* **409** 3472–81

Andela N *et al* 2017 A human-driven decline in global burned area *Science* **356** 1356–62

Andela N and van der Werf G R 2014 Recent trends in African fires driven by cropland expansion and El Niño to La Niña transition *Nat. Clim. Change* **4** 791

Archibald S *et al* 2018 Biological and geophysical feedbacks with fire in the earth system *Environ. Res. Lett.* **13** 033003

Archibald S, Nickless A, Govender N, Scholes R J and Lehsten V 2010 Climate and the inter-annual variability of fire in southern Africa: a meta-analysis using long-term field data and satellite-derived burnt area data *Glob. Ecol. Biogeogr.* **19** 794–809

Archibald S and Roy D P 2009 Identifying individual fires from satellite-derived burned area data *Proc. IGARSS* **3** 160–3

Archibald S, Roy D P, van Wilgen B W and Scholes R J 2009 What limits fire? An examination of drivers of burnt area in Southern Africa *Glob. Change Biol.* **15** 613–30

Bistinas I, Harrison S P, Prentice I C and Pereira J M C 2014 Causal relationships vs. emergent patterns in the global controls of fire frequency *Biogeosciences* **11** 5087–101

Breiman L 2001 Random forests *Mach. Learn.* **45** 5–32

Breiman L and Cutler A 2003 Setting up, using, and understanding random forests V4. 0 [online] (http://oz.berkeley.edu/users/breiman/Using_random_forest_v4.0.pdf)

Cecil D J, Buechler D E and Blakeslee R J 2015 TRMM LIS climatology of thunderstorm occurrence and conditional lightning flash rates *J. Clim.* **28** 6536–47

Cochrane M A, Alencar A, Schulze M D, Souza C M, Nepstad D C, Lefebvre P and Davidson E A 1999 Positive feedbacks in the fire dynamic of closed canopy tropical forests *Science* **284** 1832–5

Cochrane M A and Laurance W F 2002 Fire as a large-scale edge effect in Amazonian forests *J. Trop. Ecol.* **18** 311–25

Didan K 2015 MOD13C1 MODIS/terra vegetation indices 16-day L3 global 0.05Deg CMG V006 NASA EOSDIS Land Processes DAAC (https://doi.10.5067/MODIS/MOD13C1.006)

Dimiceli C, Carroll M, Sohlberg R, Kim D H, Kelly M and Townshend J R G 2015 MOD44B MODIS/terra vegetation continuous fields yearly L3 global 250m SIN grid V006 *NASA EOSDIS Land Processes DAAC* (https://doi.10.5067/MODIS/MOD44B.006)

Flannigan M D, Krawchuk M A, de Groot W J, Wotton B M and Gowman L M 2009 Implications of changing climate for global wildland fire *Int. J. Wildland Fire* **18** 483–507

Forkel M, Dorigo W, Lasslop G, Chuvieco E, Hantson S, Heil A, Teubner I, Thonicke K and Harrison S P 2019 Recent global and regional trends in burned area and their compensating environmental controls *Environ. Res. Commun.* **1** 051005

Friedl M and Sulla-Menashe D 2015 MCD12C1 MODIS/terra+aqua land cover type yearly L3 global 0.05Deg CMG V006 *NASA EOSDIS Land Processes DAAC* (https://doi.10.5067/MODIS/MCD12C1.006)

Gelaro R *et al* 2017 The modern-era retrospective analysis for research and applications, version 2 (MERRA-2) *J. Clim.* **30** 5419–54

Giglio L, Boschetti L, Roy D P, Humber M L and Justice C O 2018 The collection 6 MODIS burned area mapping algorithm and product *Remote Sens. Environ.* **217** 72–85

Giglio L, Randerson J T and van der Werf G R 2013 Analysis of daily, monthly, and annual burned area using the fourth-generation global fire emissions database (GFED4) *J. Geophys. Res. Biogeosci.* **118** 317–28

Giglio L, Schroeder W and Justice C O 2016 The collection 6 MODIS active fire detection algorithm and fire products *Remote Sens. Environ.* **178** 31–41

Guan K *et al* 2018 Simulated sensitivity of African terrestrial ecosystem photosynthesis to rainfall frequency, intensity, and rainy season length *Environ. Res. Lett.* **13** 025013

He L, Ren X, Gao Q, Zhao X, Yao B and Chao Y 2017 The connected-component labeling problem: A review of state-of-the-art algorithms *Pattern Recognit.* **70** 25–43

Hernandez C, Keribin C, Drobinski P and Turquety S 2015 Statistical modelling of wildfire size and intensity: a step toward meteorological forecasting of summer extreme fire risk *Ann. Geophys.* **33** 1495–506

Hua W, Zhou L, Chen H, Nicholson S E, Jiang Y and Raghavendra A 2018 Understanding the central equatorial African long-term drought using AMIP-type simulations *Clim. Dyn.* **50** 1115–28

Hua W, Zhou L, Chen H, Nicholson S E, Raghavendra A and Jiang Y 2016 Possible causes of the central equatorial African long-term drought *Environ. Res. Lett.* **11** 124002

Huffman G J, Bolvin D T, Nelkin E J, Wolff D B, Adler R F, Gu G, Hong Y, Bowman K P and Stocker E F 2007 The TRMM multisatellite precipitation analysis (TMPA): quasi-global, multiyear, combined-sensor precipitation estimates at fine scales *J. Hydrometeorol.* **8** 38–55

Jiang Y, Zhou L, Tucker C J, Raghavendra A, Hua W, Liu Y Y and Joiner J 2019 Widespread increase of boreal summer dry season length over the Congo rainforest *Nat. Clim. Change* **9** 617–22

Jolly W M, Cochrane M A, Freeborn P H, Holden Z A, Brown T J, Williamson G J and Bowman D M 2015 Climate-induced variations in global wildfire danger from 1979 to 2013 *Nat. Commun.* **6** 7537

Knapp K R *et al* 2011 Globally gridded satellite observations for climate studies *Bull. Am. Meteorol. Soc.* **92** 893–907

Laris P 2011 Humanizing savanna biogeography: linking human practices with ecological patterns in a frequently burned savanna of southern Mali *Ann. Assoc. Am. Geogr.* **101** 1067–88

Lasslop G and Kloster S 2017 Human impact on wildfires varies between regions and with vegetation productivity *Environ. Res. Lett.* **12** 115011

Lehmann C E R *et al* 2014 Savanna vegetation–fire–climate relationships differ among continents *Science* **343** 548–52

Malhi Y, Roberts J T, Betts R A, Killeen T J, Li W and Nobre C A 2008 Climate change, deforestation, and the fate of the Amazon *Science* **319** 169–72

Mayr M J, Vanselow K A and Samimi C 2018 Fire regimes at the arid fringe: A 16-year remote sensing perspective (2000–2016) on the controls of fire activity in Namibia from spatial predictive models *Ecol. Ind.* **91** 324–37

Nepstad D C *et al* 1999 Large-scale impoverishment of Amazonian forests by logging and fire *Nature* **398** 505–8

Nicholson S E, Klotter D, Dezfuli A K and Zhou L 2018 New rainfall datasets for the Congo Basin and surrounding regions *J. Hydrometeorol.* **19** 1379–96

Patra P K, Ishizawa M, Maksyutov S, Nakazawa T and Inoue G 2005 Role of biomass burning and climate anomalies for land–atmosphere carbon fluxes based on inverse modeling of atmospheric CO_2 *Glob. Biogeochem. Cycles* **19** GB3005

Pechony O and Shindell D T 2010 Driving forces of global wildfires over the past millennium and the forthcoming century *Proc. Natl Acad. Sci.* **107** 19167–70

Potapov P *et al* 2017 The last frontiers of wilderness: tracking loss of intact forest landscapes from 2000 to 2013 *Sci. Adv.* **3** e1600821

Raghavendra A, Zhou L, Jiang Y and Hua W 2018 Increasing extent and intensity of thunderstorms observed over the Congo Basin from 1982 to 2016 *Atmos. Res.* **213** 17–26

Randerson J T, Chen Y, van der Werf G R, Rogers B M and Morton D C 2012 Global burned area and biomass burning emissions from small fires *J. Geophys. Res. Biogeosci* **117**

Riaño D, Moreno Ruiz J A, Isidoro D and Ustin S L 2007 Global spatial patterns and temporal trends of burned area between

1981 and 2000 using NOAA-NASA pathfinder *Glob. Change Biol.* **13** 40–50
Scholes R J and Archer S R 1997 Tree–grass interactions in savannas *Annu. Rev. Ecol. Syst.* **28** 517–44
Schultz M G, Heil A, Hoelzemann J J, Spessa A, Thonicke K, Goldammer J G, Held A C, Pereira J M C and van Het Bolscher M 2008 Global wildland fire emissions from 1960 to 2000 *Glob. Biogeochem. Cycles* **22** GB2002
van der Werf G R, Randerson J T, Giglio L, Collatz G J, Mu M, Kasibhatla P S, Morton D C, Defries R S, Jin Y and van Leeuwen T T 2010 Global fire emissions and the contribution of deforestation, savanna, forest, agricultural, and peat fires (1997–2009) *Atmos. Chem. Phys.* **10** 11707–35
van der Werf G R, Randerson J T, Giglio L, Gobron N and Dolman A J 2008 Climate controls on the variability of fires in the tropics and subtropics *Glob. Biogeochem. Cycles* **22** GB3028
van der Werf G R *et al* 2017 Global fire emissions estimates during 1997–2016 *Earth Syst. Sci. Data* **9** 697–720
Westerling A L, Hidalgo H G, Cayan D R and Swetnam T W 2006 Warming and earlier spring increase western US forest wildfire activity *Science* **313** 940–3
Williams E, Rothkin K, Stevenson D and Boccippio D 2000 Global lightning variations caused by changes in thunderstorm flash rate and by changes in the number of thunderstorms *J. Appl. Meteorol.* **39** 2223–30
Yates C P, Edwards A C and Russell-Smith J 2009 Big fires and their ecological impacts in Australian savannas: size and frequency matters *Int. J. Wildland Fire* **17** 768–81
Zhou L *et al* 2014 Widespread decline of Congo rainforest greenness in the past decade *Nature* **509** 86